Exploring a critical diameter for thermo-acoustic instability of downward propagating flames in tubes

Ajit Kumar Dubey[1,2,3], Yoichiro Koyama[1], Nozomu Hashimoto[1], and Osamu Fujita[1].

[1] Division of Mechanical and Space Engineering, Hokkaido University, Kita 13 Nishi 8 Kita-ku, Sapporo, Hokkaido, 060-8628, Japan

[2] RACMaS - Research Alliance Center for Mathematical Sciences, Tohoku University

6-3 Aoba, Aramaki, Aoba-ku, Sendai, Miyagi 980-8578 Japan

[3] Institute of Fluid Science, Tohoku University, 2-1-1 Katahira, Aoba, Sendai, Miyagi 980-8577, Japan.

Corresponding author: Osamu Fujita

Division of Mechanical and Space Engineering, Hokkaido University, Kita 13 Nishi 8 Kita-ku, Sapporo, Hokkaido, 060-8628, Japan

TEL: +81-11-706-6385

FAX: +81-11-706-7841

E-mail: ofujita@eng.hokudai.ac.jp

Colloquium: LAMINAR FLAMES

Total length of paper: 6188 words

Method of determination: Method 1

Main text: 3357 words

Equation 1: 23 words

References: 577 words (31 references)

Figure 1: 132.6 words

Figure 2: 509.8 words

Figure 3: 390.8 words

Figure 4: 192.3 words

Figure 5: 151.9 words

Figure 6: 175 words

Figure 7: 147.6 words

Figure 8: 147 words

Table 1: 370.8 words

(Subtotal of figures: 1848.9 words)

Abstract

Thermo-acoustic oscillations are observed when a flame ignited at open end of a tube propagates towards the closed end due to interaction between unsteady heat release rate fluctuations from flame and acoustic fluctuations. In our past work, it was found that thermo-acoustic instability increases with decreasing diameter from 7.0 cm to 3.0 cm. A recent study in flame propagation in Hele-Shaw cells showed that thermo-acoustic instability is not observed for plate separation less than 0.4 cm. Thermoacoustic instabilities can't be observed in very narrow tubes due to excessive damping from the wall. This opens up the possibility of a critical diameter where thermo-acoustic instability would be maximum. In this work we perform flame propagation experiments with diameter of combustion tube in the range 0.5 cm to 3 cm for a fixed length of 70.2 cm. It was found that thermo-acoustic parametric instability begins at lowest laminar burning velocity when the diameter is around 1.0 cm. This diameter is termed as critical diameter. Critical diameter is found to be independent of Lewis number of mixtures. Existence of a critical diameter is thus proved experimentally. Growth rates of primary instability increase with decreasing diameter and show a maximum around the critical diameter and decrease with further decrease in tube diameter. But, growth rates of secondary instability as well as maximum pressure fluctuation amplitude decreases continuously with decreasing diameter. Mechanisms responsible for these observations and existence of a critical diameter are clarified.

Keywords: Lewis number, acoustic parametric instability, primary acoustic instability, Effect of geometrical parameters, Growth rates

1. **Introduction**

Thermo-acoustic oscillations have adverse effects on operation of many combustion devices [1]. These oscillations occur due to coupling between unsteady heat release rate fluctuations from flame and acoustic fluctuations and are also cause of some flame front instabilities [2]. A simple experiment to understand the thermo-acoustic instability with premixed flame as heat source is a downward propagating flame in tube open at ignition end which was demonstrated by Searby [3]. The flame ignited at open end usually evolves into a curved flame front with various cells. The size of these cells depends on hydrodynamic and thermo-diffusive instabilities. As this flame travels down, flame and acoustic oscillations begin, and amplitudes of the flame cells decrease which can transition to a vibrating flat flame. This regime of acoustic instability is called primary instability. If the mixture strength is high enough, corrugations of a particular wavenumber develop on this flat flame front which leads to a turbulent fluctuating flame accompanied by a high amplitude pressure oscillation. This is termed as secondary acoustic instability. The corrugated structure is due to parametric instability of flame front in the acoustic field [4] and is the cause of secondary instability [5]. This parametric instability has been studied analytically for planar flame [6] fronts and also extended to spherical flames [7] and triple flames [8]. For much stronger mixture, there is no transition to flat flame and initial curved flame directly transitions to secondary instability leading to “complete instability” of a flat flame in acoustic field [9]. Higher modes of parametric instability can be observed with even stronger mixtures [5]. Pressure coupling [10][11][12] and velocity coupling [13] has been proposed to understand the mechanism of instability and predict its growth rate. In pressure coupling, the unsteady heat release rate oscillations are generated by the fluctuations of pressure at flame front which creates fluctuations in final temperature. In velocity coupling, those oscillations are generated by change in area of the flame front. Primary instability growth rate can be successfully predicted using velocity coupling [14]. Secondary instability has larger growth rates and maximum pressures compared to primary instability. The phenomena of primary and secondary instability had also been studied using

large activation energy asymptotic theory of flame coupled with acoustics [15] and some aspects of experiments can be reproduced by considering weakly non-linear coupling between flame and eigen modes of tube [16].

Onset of primary instability [17] and parametric instability [18][19] has also been studied in downward propagating flames using laser irradiation technique which sheds light on turbulization mechanism of flat flame [20][21]. Effect of Lewis number (*Le*) on primary [22] and secondary instability [5][19] shows that lower *Le* mixtures are more prone to instability. Thermoacoustic instabilities were also studied in annular space [23] and Hele-Shaw cells [24] to understand effect of Markstein number. Thermoacoustic instabilities in highly reactive H_2/air mixtures were also studied [25][26]. Open ended tubes [27] also show oscillating flames due to interaction with acoustics. Owing to continuous efforts in the last few decades a lot is now known about the thermoacoustic instabilities during propagating flame experiments.

The instability in combustion tubes depends on the geometric parameters. Clavin et al. [10] first studied the influence of geometrical parameters analytically based on pressure coupling mechanism and predicted that shorter and wider tubes will be more unstable. Effect of geometrical parameters were experimentally investigated, and contrary to pressure coupling predictions, it was found that longer (in the range 300 to 700 mm) and narrower tubes (diameter changed from 30 to 70 mm) were more unstable [28]. It was also proved that velocity coupling mechanism could successfully explain such results [28]. Effect of length on instability is monotonic i.e. decreasing length increases the acoustic loss and thus instability is decreased. However, effect of diameter is interesting and necessarily non-monotonic. Numerical study on flame oscillation in 2-D open channels showed that flame oscillations increases with increase in channel width in the range of 20 to 120 times the flame thickness which roughly corresponds to width of order of a millimeter [29]. Numerical simulation of flame traveling from open to closed end in a 2-D channel has also been performed by considering flame-acoustic coupling which captures violent folding of flame front similar to parametric instability [30] and it was also found that oscillations are stronger in wider tubes

[31]. However, the scales of these simulations are much smaller than reported experiments [30-31]. Recent experiments on oscillatory flame propagation in Hele-Shaw cells found that pressure oscillations were not observed for channel width of 4 mm or lower but oscillation increased when width was increased from 7 to 10 mm [24]. Naturally, thermoacoustic instability cannot happen in very narrow tubes due to drastic decrease in flame propagation effected by increased heat losses to the walls leading to flammability limits and effects of increased acoustic losses. Hence, it seems logical that there would exist a critical diameter of tube for which thermo-acoustic instability would be maximized.

Current work fills this gap in information with experimental investigations to find a critical diameter for thermo-acoustic instability in downward propagating flames in tubes. Effect of properties of combustible mixture on this critical diameter is also assessed. Effect of diameter on various aspects of thermoacoustic instability is discussed.

2. Experimental method

The schematic of experimental setup is shown in Fig. 1. The combustion tube is a transparent acrylic tube which was fixed vertically. The tube was closed at bottom and a lid was fixed on the upper side which can be opened by the action of an electromagnet.

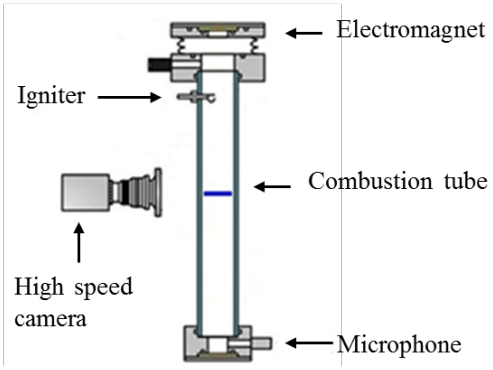

Fig.1. Schematic of experimental setup.

The combustion tube is a vertically fixed transparent acrylic tube. the diameter of combustion tube was varied from 0.5 to 3.0 cm for a fixed length of 70.2 cm. $C_2H_4/O_2/CO_2$ mixtures of equivalence ratio 0.8 and 1.2 as well as $C_2H_4/O_2/N_2$ mixtures at equivalence ratio 0.8 were used for which Lewis number, *Le* based on deficient reactant was 1.05, 0.8 and 1.34 respectively. The mixture was filled in the combustion tube at atmospheric pressure. CO_2 and N_2 dilution were varied to vary laminar burning velocity (S_L) of mixtures. The mixture conditions and properties are tabulated in Table 1. After the mixture became quiescent, the upper lid was opened by action of an electromagnet and simultaneously the mixture was ignited at the open end. So, during the flame propagation the tube had one end open and another end closed. The flame propagation is recorded using a high-speed camera FASTCAM at 1000-2000 frames per second. The pressure fluctuations are measured using a PCB Piezotronics 106B52 dynamic pressure sensor at the bottom of the tube at sampling rate of 10 kHz.

Table 1. Mixture composition and properties

C_2H_4 (%)	O_2 (%)	CO_2 (%)	S_L (cm/s)	φ	*Le*	T_b (K)	α (cm^2/s)
7.03	17.57	75.4	**7.59**	1.2	0.784	1707	0.1267302
7.46	18.64	73.9	**9.99**		0.787	1786	0.1276422
7.85	19.64	72.51	**12.49**		0.79	1858	0.1283348
8.21	20.52	71.28	**14.99**		0.792	1922	0.1290639
8.54	21.35	70.12	**17.51**		0.795	1982	0.1297316
5.06	18.99	75.95	**7.34**	0.8	1.042	1626	0.128039
5.45	20.43	74.12	**10.04**		1.045	1717	0.1291445
5.75	21.56	72.7	**12.51**		1.048	1787	0.1300289
6.02	22.58	71.4	**15**		1.05	1850	0.130845
6.28	23.56	70.16	**17.51**		1.052	1907	0.1316052
6.52	24.44	69.04	**20**		1.054	1957	0.13234
6.74	25.28	67.98	**22.5**		1.056	2002	0.133065
C_2H_4 (%)	**O_2 (%)**	**N_2 (%)**	**S_L (cm/s)**		***Le***	**T_b (K)**	**α (cm^2/s)**
3.27	12.25	84.48	**9.97**	0.8	1.353	1579	0.2151825
3.45	12.95	83.6	**12.49**		1.351	1639	0.2149154
3.61	13.53	82.86	**14.99**		1.35	1692	0.2147467
3.76	14.12	82.13	**17.5**		1.348	1742	0.214445
3.91	14.65	81.44	**20.02**		1.346	1787	0.2141339
4.04	15.15	80.82	**22.5**		1.345	1830	0.213975
4.16	15.62	80.22	**24.99**		1.343	1869	0.2137145
4.29	16.09	79.62	**27.5**		1.342	1908	0.21351

3. Results and discussion

3.1. Flame regimes: Effect of *Le*

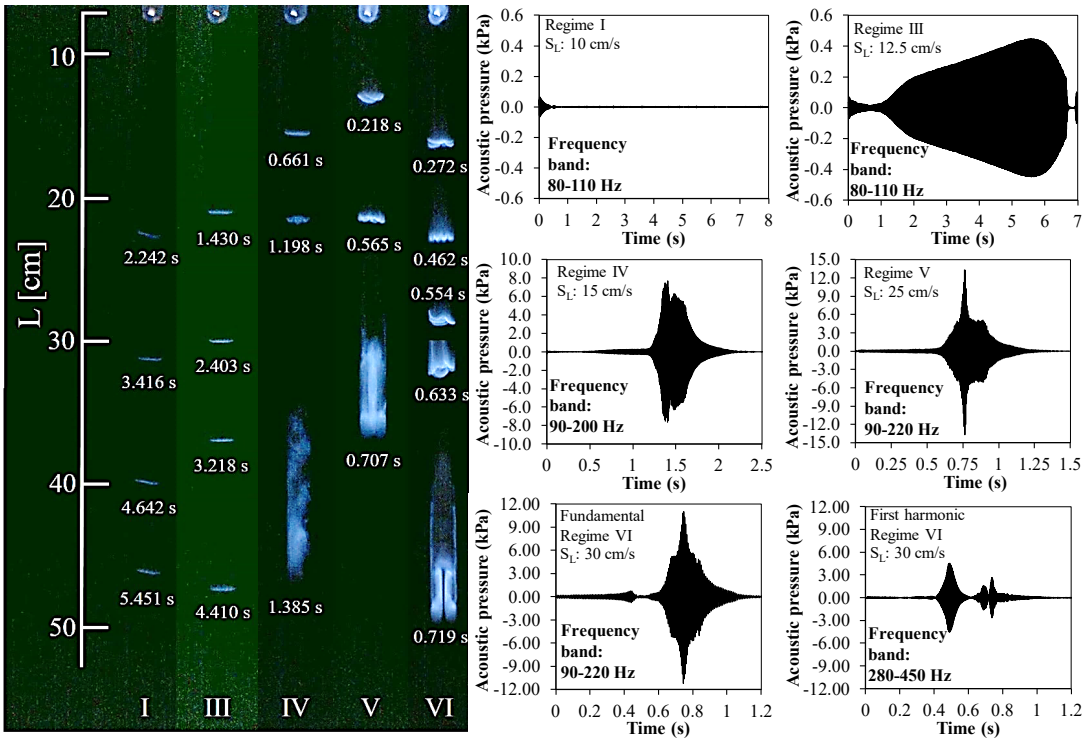

Fig.2. Representative images for the observed flame responses and corresponding pressure history (L=70.2 cm, D=20 mm) for *Le*=1.05 mixtures. Time instant of flame image is measured from beginning of ignition. The frequency bands for pressure oscillations after FFT are also shown.

Figure 2 shows representative images at different stages of downward propagation for various flame responses observed in present experiments along with associated pressure history for each regime in tube of inner diameter 20 mm for *Le*=1.05 mixtures. The pressure fluctuations show a peak in frequency near the fundamental acoustic mode of the tube and also first harmonic mode of the tube for Regime VI. The spectral plots are not shown here due to space limits but are very similar to ones presented in our earlier works [5][9]. The frequency bands for shown pressure fluctuations are mentioned in Fig. 2. The regime names are assigned to be consistent with our earlier works [5][28]. Typical flame dynamics for each of the observed flame responses is described first and is qualitatively similar to the responses observed at

larger diameters. The overall variations in flame responses due to change in *Le*, S_L and diameter are presented later. Mixtures with S_L lower than 8 cm/s could not have a propagating flame and extinguished soon after ignition. During regime I, a curved flame propagates steadily downwards, and no thermoacoustic instability is observed as is evident from the pressure history of regime I which shows no pressure fluctuations. During regime II [22], a vibrating curved flame propagates upon ignition, but is not observed for low diameter tubes of current work. During regime III, thermoacoustic instability is generated and initial cellular flame starts vibrating after propagating some distance; this vibrating cellular flame transitions to a vibrating flat flame during primary acoustic instability where pressure amplitudes increase as the flame propagates further downward. The flame also vibrates at the acoustic frequency. The vibrating flat flame then propagates to the end of tube and pressure fluctuations increase at a growth rate lower than the initial growth rate. The possible reason for decrease in growth rate will be discussed now. During the transition from cellular flame to vibrating flat flame there is change in flame area over each oscillation so velocity coupling is the main mechanism for instability. After the flame turns flat there is no change in the flame are which indicates that velocity coupling cannot have a role and pressure coupling is the only possible mechanism. Pressure coupling produces much weaker coupling with growth rates predicted to be at least an order of magnitude lower than the velocity coupling [14]. Thus, lower growth rates are observed after flame turns flat. During regime IV, a cellular flame transitions to a flat flame which transitions to turbulent and inhomogeneous oscillating flame via corrugated structures on flame front due to parametric instability. Pressure increases first then saturates and then increases at a much higher rate when parametric instability is generated. During regime V, initial curved flame with soft cells propagates downward after ignition and amplitude of the flame cells reduces due to primary acoustic instability. Thereafter, corrugated structures are formed on the curved flame due to parametric instability leading to fluctuating turbulent flame. In contrast with regime IV, flat flame is never formed in regime V. Regime VI shows higher modes of acoustic parametric instability, where parametric instability of first

harmonic is observed in upper half of tube which transforms into parametric instability of fundamental mode around middle of tube. This can be observed from the pressure fluctuations which are shown for two frequency ranges. More about higher modes can be learned from our earlier work [5].

Experiments are performed for *Le* of 1.34, 1.05 and 0.8 for different diameters and S_L and Fig. 3 shows the summary of observed flame responses. Four distinct regions i.e. non-propagating flame, stable propagating flame without thermoacoustic instability, flame with primary acoustic instability and flame with secondary acoustic instability are shown are shown in Fig. 3. The instability of the flame increases with increase in S_L for all *Le* and diameter cases. The minimum S_L for primary instability doesn't change with diameter of tube for *Le* =0.8 and 1.05 but for *Le* =1.34, the minimum S_L is observed for diameter of 10 mm. However, minimum S_L for the onset of secondary instability clearly shows a minimum around 10 mm for all *Le*. Hence, the onset of secondary instability is more affected by the change in diameter as compared with onset of primary instability.

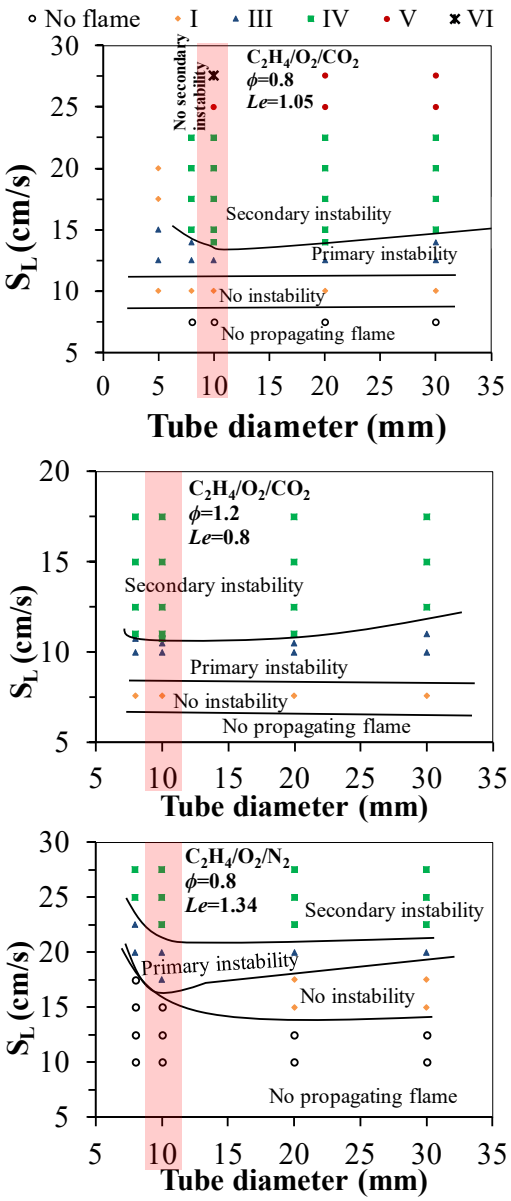

Fig.3. Summary of flame responses observed for different *Le* mixtures. Markers are experimental results. The curves represent approximate boundaries between two stability regimes. Flame responses at critical diameter are shaded.

The minimum S_L for primary and secondary instability decreases with *Le* for any diameter. First, we consider minimum S_L for primary instability which is primarily decided by temperature ratio. For clarification, consider the case of D=8 mm. S_L at onset of primary instability is 10, 12.5 and 20.0 for *Le*=0.8, 1.05 and 1.34 respectively. Adiabatic flame temperature is same (1787 K) for these three mixtures

and the initial mixture temperature is also same. Hence, the onset of primary instability is evidently governed by the temperature ratio. This is consistent with theoretical understanding as the temperature ratio is a factor in the transfer function for velocity coupling used to calculate growth rate of primary instability [14]. Similar observations were made in our last work where onset of primary instability was always observed at 12.5 cm/s for *Le*=1.05 when diameter of tube was changed from 3 cm to 7 cm [28]. The onset of secondary instability is governed by amplitude of acoustic perturbations as will be discussed in next section. Importantly, the minimum S_L for primary instability (*Le*=1.34) and secondary instability irrespective of *Le* is always observed with 10 mm diameter tube. It can be observed that the overall tendency to induce thermoacoustic instability is maximized i.e. stronger parametric instability is generated for mixtures with lowest S_L when diameter of tube is around 10 mm which can be termed as a critical diameter. This also means that parametric instability is generated for maximum range of fuel-fractions or mixture conditions at critical diameter. Also, this critical diameter is not much affected by *Le* but this is not to say that *Le* has no effect on thermoacoustic instability. For e.g., the minimum S_L at which primary instability is generated depends on the mixture properties as already discussed. Also, effect of *Le* on primary acoustic instability, growth rates of secondary instability [5] and boundary of Regime V [9] has been assessed in our earlier works. The critical diameter is influenced more by the acoustic losses which depends largely on geometrical parameters as is discussed later. This is the first work to demonstrate the existence of a critical diameter for thermoacoustic instability. For tube diameter of 5 mm with *Le*=1.05, no secondary instability was observed. Secondary instability was not observed for tube diameter of 8 mm at S_L above 22.5 cm. Parametric instability phenomenon has newer manifestations for tubes below critical diameter and will be taken up in our future work.

Here, it also seems important to mention the numerical results of [31] about effect of width of channel on amplitude of oscillations. Interestingly, the amplitude of oscillations shows a maximum (Fig. 14 of [31]) when tube width is varied which is conceptually similar to existence of a critical diameter found in this

work even though the geometric scales and mixtures are too different for a direct comparison. However, the more important eigen mode in their simulations is one between flame front and closed end of tube whereas in experiments the important eigen mode is related to total length of tube. Also, effect of *Le* predicted by their simulations is generally not consistent with experiments where lower *Le* mixtures show higher growth rates.

3.2. Effect of diameter on flame dynamics and thermoacoustic instability

To illustrate further on the effect of tube diameter, *Le*=1.05 mixtures are considered. First the effect of diameter on primary acoustic instability is discussed. The minimum S_L at onset of primary instability doesn't change with diameter as we saw in last section. However, effect of diameter is clear if we consider the growth rates of primary instability shown in Fig. 4. The growth rates are calculated by fitting the experimental data of pressure oscillations using $p = A\exp\left(\frac{t}{\tau_{ins}}\right)\cos(\omega t + \varphi)$, here $\frac{1}{\tau_{ins}}$ is the growth rate of instability, p is pressure, ω is circular frequency, t is time, A is amplitude of pressure oscillation, φ is phase. The growth rate increases with decreasing diameter of tube and shows a maximum at diameter of 8 mm or 10 mm depending on S_L. For velocity coupling, the growth rate of primary instability depends on the wavenumbers of cellular structure near the onset of primary instability. Figure 4 also shows the images at onset of primary instability for various tube diameters. It can be seen that the wavenumber of cells increases with decreasing diameter of tube because the cell sizes decrease. For tube diameter of 8 to 20 mm a single curved front is observed, the wavenumber of which is solely decided by the diameter of the tube. For tube diameter of 30 mm more than one cell is observed with the lowest wavenumber associated with a cell encompassing the whole diameter. Due to increase in wavenumber of cells the growth rate of primary instability increases with decreasing diameter before dropping significantly for diameter of 5 mm as is shown in Fig.4.

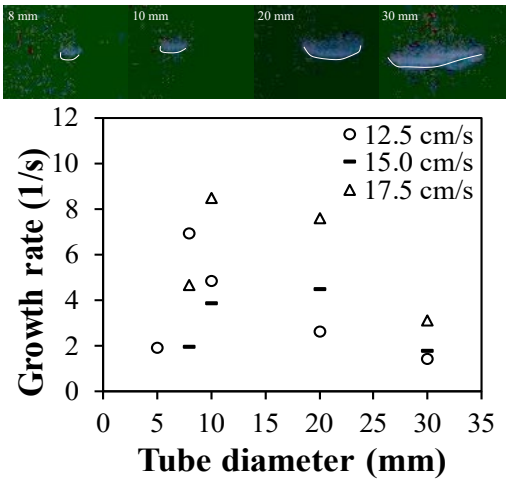

Fig.4. Flame images showing wavenumber at onset (top) and growth rate (bottom) of primary instability at all diameters. Flame front contour is artificially drawn to clearly indicate the change in wavenumber.

This drop in growth rate of primary instability at low diameter is due to acoustic losses which increase significantly with decreasing diameter of tube as is shown in Fig. 5. Total acoustic loss ($\frac{1}{\tau_{loss}}$) comprises of wall losses ($\frac{1}{\tau_{wall}}$) due to acoustic boundary layer which impedes the acoustic perturbations and radiation losses ($\frac{1}{\tau_{rad}}$) from the open end and is given by following equation [14]

$$\frac{1}{\tau_{loss}} = \frac{1}{\tau_{wall}} + \frac{1}{\tau_{rad}} = \sqrt{8}\frac{(\omega\alpha)^{1/2}}{D}[(\gamma-1)/\sqrt{\gamma}+\sqrt{Pr}] + \frac{1}{8}\frac{(\omega D)^2}{cL} \quad (1)$$

Here, ω is acoustic circular frequency, α is thermal diffusivity, γ is ratio of specific heats (1.4), Pr is Prandtl number (0.72), c is speed of sound in the gas (267 m/s); D is diameter and L is length of tube (702 mm). Total losses are dominated by the wall losses for current length of tube. Hence, even though radiation losses decrease with decreasing diameter, the increase in wall losses due to decreasing diameter makes up for it and total losses increase.

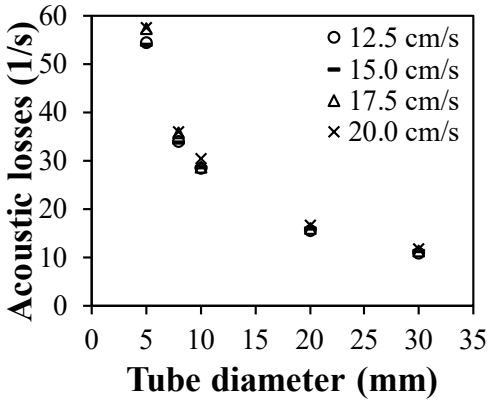

Fig.5. Variation of acoustic losses with tube diameter calculated using Eqn. 1.

Proper structures at the onset of parametric instability are not observed for tube diameter below 10 mm. Importantly, wavenumber of structures at onset of parametric instability are independent of diameter. Onset of parametric instability happens at a particular wavenumber when the acoustic pressure is higher than a minimum value which is decided by frequency of oscillation and mixture properties [4].

The pressure amplitude at the onset of parametric instability with various tube diameters were assessed and it was found that it isn't highly affected by tube diameter (Fig. 6). Small variations within 0.1 kPa are observed. So, the parametric instability begins when the acoustic pressure amplitude reaches a required value. Now we can understand why onset of parametric instability begins at lower S_L in lower diameter experiments. This is because the growth rate of primary instability is higher at lower diameter hence the pressure increases faster and the acoustic pressure necessary for parametric instability is reached at lower S_L. In current experiments the length of tube is constant, so the frequency of acoustic oscillations is almost constant. Also, if we consider same mixture the wavenumber at onset of parametric instability is invariant with diameter. There will be some secondary effect of diameter because at considerably low diameter heat loss reduces the burning velocity which can affect the wavenumber. However, before reaching that diameter which is affected by heat loss if the diameter of tube becomes lower than the particular wavenumber then parametric instability may not be observed. Considering the current mixtures of *Le*=1.05, the wavelength of structures on flame front at the onset of parametric instability is near 0.5 cm

as can be calculated using theory presented in [4]. Hence, below 1 cm it could become difficult to observe the parametric instability with proper corrugated structures. It can be seen from flame images of regime VI in Fig.2 that only one or two corrugations are observed during turbulent flame propagation.

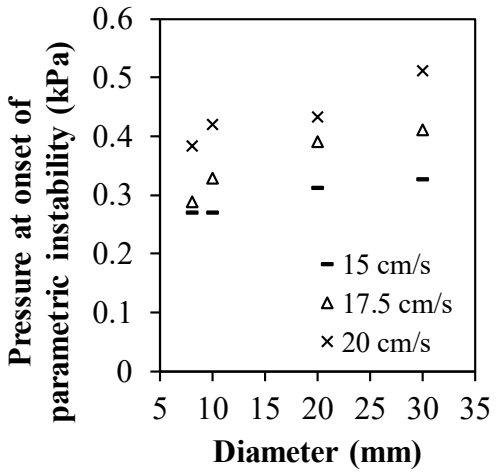

Fig.6. Pressure at onset of parametric instability at all diameters.

As the total acoustic losses increase with decrease in diameter, the growth rate of secondary instability reduces when diameter is decreased. This trend is observed in Fig. 7. Growth rate of secondary instability is calculated in same manner as our previous work by taking the envelope of amplitudes of pressure fluctuations and fit an exponential curve $p = A \exp\left(\frac{t}{\tau_{ins}}\right)$ because frequency varies during parametric instability due to sudden rise in temperature [5]. Now, it is clear why primary and secondary instability growth rates show opposite tendency with variation in diameter. Figure 8 shows how maximum amplitude pressure oscillations change with diameter. The maximum pressure increases as the tube diameter is increased from 5 to 30 mm. Unlike the minimum S_L, the maximum pressure doesn't show a maximum at critical diameter.

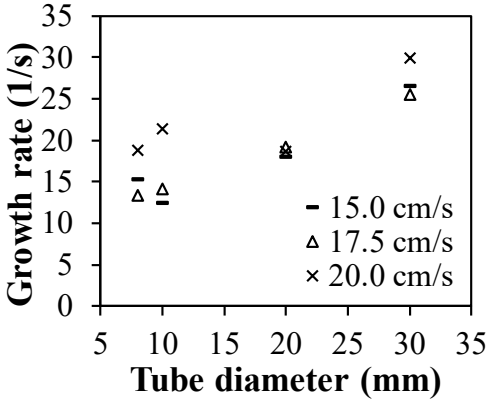

Fig.7. Growth rate of secondary instability at all diameters.

Maximum pressure increases with increase in tube diameter which is due to stronger secondary instability with decreased acoustic loss. This also reflects in the secondary instability growth rate which generally increases with increasing tube diameter.

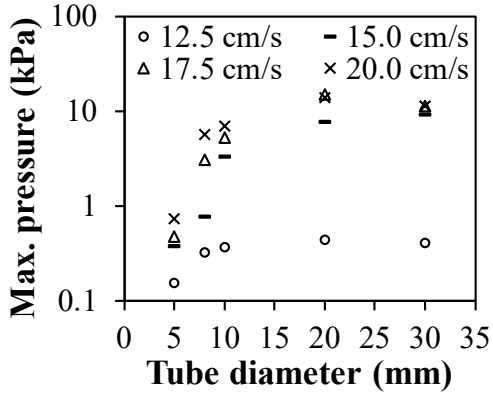

Fig.8. Maximum pressure amplitude during instability at all diameters.

4. Conclusion

Existence of a critical diameter where secondary instability of downward propagating flames is observed at minimum S_L was shown experimentally. This critical diameter was found to be around 10 mm for three set of mixtures used here. Interestingly, unlike other aspects of thermoacoustic instability e.g. growth rates, the critical diameter doesn't depend much on *Le* of the mixtures. However, S_L of mixture at which instability begins at every diameter is higher for higher *Le* mixtures. Growth rates of primary acoustic

instability shows a maximum near the critical diameter whereas growth rates of secondary instability and maximum amplitude of pressure fluctuations increase with diameter. The mechanisms of these observed phenomena are clarified.

Acknowledgements

This study was supported by a Grant-in-Aid for Scientific Research KIBAN(A)#18H03755 from MEXT Japan.

References

[1] T. Poinsot, Prediction and control of combustion instabilities in real engines, Proc. Combust. Inst. 36 (2017) 1–28.

[2] P. Clavin, Dynamics of combustion fronts in premixed gases: From flames to detonations, Proc. Combust. Inst. 28 (2000) 569–585.

[3] G. Searby, Acoustic Instability in Premixed Flames, Combust. Sci. Technol. 81 (1992) 221–231.

[4] G. Searby, D. Rochwerger, A parametric acoustic instability in premixed flames, J. Fluid Mech. 231 (1991) 529–543.

[5] A. K. Dubey, Y. Koyama, N. Hashimoto, O. Fujita, Experimental and theoretical study of secondary acoustic instability of downward propagating flames: Higher modes and growth rates, Combust. Flame 205 (2019) 316–326.

[6] V. Bychkov, Analytical scalings for flame interaction with sound waves, Phys. Fluids, 11 (1999) , 3168–3173.

[7] V. 'yacheslav Akkerman, C. K. Law, Effect of acoustic coupling on power-law flame acceleration in spherical confinement, Phys. Fluids, 25 (2013) , 013602.

[8] V. 'yacheslav Akkerman, C. K. Law, Coupling of harmonic flow oscillations to combustion instability in premixed segments of triple flames, Combust. Flame 172 (2016) 342–348.

[9] A. K. Dubey, Y. Koyama, S. H. Yoon, N. Hashimoto, O. Fujita, Range of "complete" instability of flat flames propagating downward in the acoustic field in combustion tube: Lewis number effect, Combust. Flame 216 (2020) 326–337.

[10] P. Clavin, P. Pelcé, L. He, One-dimensional vibratory instability of planar flames propagating in tubes, J. Fluid Mech. 216 (1990) 299–318.

[11] P. Clavin, G. Searby, Unsteady response of chain-branching premixed-flames to pressure waves, Combust. Theory Model. 12 (2008) 545–567.

[12] A. C. Mcintosh, Pressure disturbances of Different Length Scales Interacting with Conventional Flames, Combust. Sci. Technol. 75 (1991) 287–309.

[13] P. Pelcé, D. Rochwerger, Vibratory instability of cellular flames propagating in tubes, J. Fluid Mech. 239 (1992) 293–307.

[14] C. Clanet, G. Searby, P. Clavin, Primary acoustic instability of flames propagating in tubes: cases of spray and premixed gas combustion, J. Fluid Mech. 385 (1999) 157–197.

[15] X. Wu, M. Wang, P. Moin, N. Peters, Combustion instability due to the nonlinear interaction between sound and flame, J. Fluid Mech., (2003) .

[16] R. C. Assier, X. Wu, Linear and weakly nonlinear instability of a premixed curved flame under the influence of its spontaneous acoustic field, J. Fluid Mech, 758 (2017) , 180–220.

[17] S. H. Yoon, T. J. Noh, O. Fujita, Onset mechanism of primary acoustic instability in downward-propagating flames, Combust. Flame 170 (2016) 1–11.

[18] Y. Taniyama, O. Fujita, Initiation and formation of the corrugated structure leading to the self-turbulization of downward propagating flames in a combustion tube with external laser absorption, Combust. Flame 161 (2014) 1558–1565.

[19] Y. Chung, O. Fujita, N. Hashimoto, Effect of Le on criteria of transition to secondary acoustic instability of downward-propagating flame in a tube with controlled curvature induced by external laser, Proc. Combust. Inst. 37 (2019) 1887–1894.

[20] M. Tsuchimoto, O. Fujita, T. Honko, Y. Nakamura, H. Ito, Research on the relation of flame front curvature and oscillatory flame propagation by external laser irradiation method, Proc. Combust.

Inst. 32 (2009) 1003–1009.

[21] J. S. Park, O. Fujita, Y. Nakamura, H. Ito, Transition of flat flames to turbulent motion induced by external laser irradiation, Proc. Combust. Inst. 33 (2011) 1105–1112.

[22] S. H. Yoon, T. J. Noh, O. Fujita, Effects of Lewis number on generation of primary acoustic instability in downward-propagating flames, Proc. Combust. Inst. 36 (2016) 1603–1611.

[23] R. C. Aldredge, N. J. Killingsworth, Experimental evaluation of Markstein-number influence on thermoacoustic instability, Combust. Flame 137 (2004) 178–197.

[24] F. Veiga-López, D. Martínez-Ruiz, E. Fernández-Tarrazo, M. Sánchez-Sanz, Experimental analysis of oscillatory premixed flames in a Hele-Shaw cell propagating towards a closed end, Combust. Flame 201 (2019) 1–11.

[25] J. Yanez, M. Kuznetsov, J. Grune, Flame instability of lean hydrogen–air mixtures in a smooth open-ended vertical channel, Combust. Flame 162 (2015) 2830–2839.

[26] J. Yáñez, M. Kuznetsov, R. Redlinger, The acoustic–parametric instability for hydrogen–air mixtures, Combust. Flame 160 (2013) 2009–2016.

[27] J. Yang, F. M. S. Mossa, H. W. Huang, Q. Wang, R. Woolley, Y. Zhang, Oscillating flames in open tubes, Proc. Combust. Inst. 35 (2015) 2075–2082.

[28] A. K. Dubey, Y. Koyama, N. Hashimoto, O. Fujita, Effect of geometrical parameters on thermo-acoustic instability of downward propagating flames in tubes, Proc. Combust. Inst. 37 (2019) 1869–1877.

[29] V. ’yacheslav Akkerman, V. Bychkov, A. Petchenko, L.-E. Eriksson, Flame oscillations in tubes with nonslip at the walls, Combust. Flame 145 (2006) 675–687.

[30] A. Petchenko, V. Bychkov, V. ’yacheslav Akkerman, L.-E. Eriksson, Violent Folding of a Flame

Front in a Flame-Acoustic Resonance, Phys. Rev. Lett. 97 (2006) 164501..

[31] A. Petchenko, V. Bychkov, V. ’yacheslav Akkerman, L.-E. Eriksson, Flame-sound interaction in tubes with nonslip walls, Combust. Flame 149 (2007) 418–434.

List of tables captions

Table 1. Mixture composition and properties.

List of figures captions

Figure 1. Schematic of experimental setup.

Fig.2. Representative images for the observed flame responses and corresponding pressure history (L=70.2 cm, D=2 cm). Time instant of flame image is measured from beginning of ignition. The frequency bands for pressure oscillations after FFT are also shown.

Fig.3. Summary of flame responses observed for different *Le* mixtures. Markers are experimental results. The curves represent approximate boundaries between two stability regimes. Flame responses at critical diameter are shaded.

Fig.4. Flame images showing wavenumber at onset (top) and growth rate (bottom) of primary instability at all diameters. Flame front contour is artificially drawn to clearly indicate the change in wavenumber.

Fig.5. Variation of acoustic losses with tube diameter calculated using Eqn. 1.

Fig.6. Pressure at onset of parametric instability at all diameters.

Fig.7. Growth rate of secondary instability at all diameters.

Fig.8. Maximum pressure amplitude during instability at all diameters.